

# Improved Cardiac Tagging Resolution at Ultra-High Magnetic Field Elucidates Transmural Differences in Principal Strain in the Mouse Heart and Reduced Stretch in Dilated Cardiomyopathy

Janusz H. Hankiewicz and E. Douglas Lewandowski

Program in Integrative Cardiac Metabolism, Center for Cardiovascular Research, University of Illinois at Chicago College of Medicine, Chicago, Illinois, USA

## ABSTRACT

Cardiac tagging resolution for regional principal strains E1 and E2 has been a limiting factor for the study of dilated mouse hearts, in which the left ventricle (LV) wall thickness can drop to below 1 mm. Therefore, high resolution tagging was performed at 14.1 T to enable transmural principal strain measurements across the LV wall of normal mouse hearts and average principal strains in thinned LV walls of a transgenic mouse (PKC $\epsilon$  TG) that develops dilated LV. A modified DANTE tagging and fast gradient imaging method produced a tagging grid dimension of  $0.33 \times 0.33$  mm and line thickness under 0.1 mm. In normal mice, average E1 strain in the epicardium was significantly higher than the endocardial E1 (epi =  $0.22 \pm 0.10$ ; endo =  $0.13 \pm 0.07$ ,  $p < 0.05$ ), while magnitude of average endocardial E2 was greater than in the epicardium (endo =  $-0.12 \pm 0.03$ , epi =  $-0.08 \pm 0.03$ ;  $p < 0.001$ ). E1 strain averaged over four segments was reduced in dilated hearts compared to controls (PKC $\epsilon$  TG =  $0.14 \pm 0.02$ ; control =  $0.18 \pm 0.02$ ,  $p < 0.01$ ), with specific reductions in septal (33%) and lateral (31%,  $p < 0.01$ ) segments. E2 strain was similar between dilated and control hearts at  $-0.11 \pm 0.01$ . Thus, improved tagging resolution demonstrates that stretch (E1), but not compression strains (E2), are reduced as a result of significant LV wall thinning in a mouse model of dilated cardiomyopathy.

## INTRODUCTION

Among many noninvasive modalities available for the study of murine hearts, cardiovascular MR has been proven to be the most suitable. It offers a unique combination of high spatial and temporal resolution needed for quantification of left ventricular volumes and mass, and assessment of global and regional myocardial wall mechanics in small sized (8–10 mm) and fast

beating (500–600 bpm) mouse hearts. Two dimensional cardiac tagged imaging has been applied successfully to the study of normal (1, 2) and infarcted (3, 4) mouse hearts. To date, published MRI studies of *in vivo* mouse hearts have provided circumferential twist and strain measurements from a tagging grid on the order of  $0.6 \times 0.6$  mm to  $1.2 \times 1.2$  mm with tag line thicknesses ranging 0.16–0.2 mm (1, 2, 5–7). However, resolution of the tagging grid has been a significant limitation for determining strain across the pathologically thinned, left ventricular wall of the mouse heart.

Strains reflect the relative motion of points within the myocardium and are determined by the displacement of triangular elements bounded to intersecting tag lines. If tagging line separation is of the order of myocardial wall size, then 2D strain analysis weights the data at mid-wall due to loss of the tag intersections and associated triangles at or beyond the endocardial and epicardial layers. Although phase displacement encoded measurements of strains have been performed on the epi- and endo-cardial layers of mouse hearts using DENSE methods (8, 9), to date, differentiating endo- and epi-cardial strains in the mouse heart left ventricle (LV) using tagging methods has not been feasible. Furthermore, previous limitations in tagging

Received 15 February 2007; accepted 9 August 2007.

Keywords: Myocardium, MR Tagging, Wall Thinning, Transmural, Left Ventricle.

This work was supported, in part, by National Institutes of Health Grants RO1HL62702 and R37HL49244. Dr. Xin Yu of Case Western Reserve University provided the strain analysis software.

Correspondence to:

E. Douglas Lewandowski, Ph.D.

Department of Physiology and Biophysics, MC901

UIC College of Medicine

835 South Wolcott Avenue

Chicago, IL 60612

tel: 312-413-7261; fax: 312-996-2870

email: dougl@uic.edu

resolution have precluded strain analysis in dilated myopathic mouse hearts, which result in progressive thinning of the LV wall to thicknesses of less than 1.0 mm.

Therefore, the goal of this study was to apply high resolution cardiac tagging for ultra-high field (14.1 T) images for the purpose of measuring regional first principal (E1) and second principal (E2) strains, in the thinned LV walls on an established mouse model of dilated cardiomyopathy (10, 11). We present significant improvements in tagging resolution at ultra-high magnetic field that enable us to distinguish transmural values for the principal strains in normal mouse hearts and to determine regional E1, E2, Err and Ecc strains in a transgenic (TG) mouse heart that develops a pure dilated cardiomyopathy.

## METHODS

### *Animal preparation*

Transmural strain measurements in LV were performed on normal, 12 month old male FVB/N mice ( $n = 4$ ). For studies of dilated hearts with thinned LV walls, protein kinase C $\epsilon$  over-expressing, transgenic (PKC $\epsilon$  TG) mice (FVB/N background,  $n = 6$ ) and age-matched, FVB/N control mice ( $n = 5$ ) were used at 9 months of age. All animals were housed under controlled temperatures, humidity and light, with normal chow and water available *ad libitum*. The protocols are approved by the Animal Care Policies and Procedures Committee at UIC (IACUC accredited), and animals were maintained in accordance with the *Guide for the Care and Use of Laboratory Animals* (National Research Council, revised 1996).

For imaging, adult mice (25–40 g) were first anesthetized with 5% Isoflurane and 100% medical grade Oxygen in an induction chamber (E-Z System, Palmer, Pennsylvania, USA). Mice were transferred to a cradle designed for a vertical bore magnet and restrained supine and light anesthesia was continued from a flow vaporizer (SurgiVet, Waukesha, Wisconsin, USA) through a custom-designed nose cone. Animals were maintained under anesthesia administered via nose cone (1% Isoflurane in 2 L/min flow of 100% O<sub>2</sub>) with spontaneous breathing throughout the 100–120 minute imaging protocol. Excess anesthetic was scavenged by a charcoal filter. Body temperature was continuously monitored rectally and maintained around 37°C by a continuous flow of warm water through Tygon tubing (1/8" OD, 1/16" ID) lining the body. The circulator was set at fast speed to prevent image ghosting from passing water. At the completion of the protocol, animals were warmed under an infra red heating and after full recovery from anesthesia (1–4 minutes) were returned to cages.

For cardiac triggering ECG platinum electrodes were subcutaneously inserted into the front right and rear left legs and connected to a monitoring device (SA Instruments Inc., Stony Brook, New York, USA). To avoid image distortion no electrode wires entered the RF coil. The monitor's control program detected the R-wave raising slope and delivered proper cardiac triggering to the spectrometer shortly before the R-wave peak appeared. Motion artifacts were reduced by res-

piratory blanking. Triggering was additionally blanked during image acquisition to prevent accidental triggering by gradients (12, 13).

### *MR imaging*

<sup>1</sup>H anatomical and tagged cardiac imaging was performed on a 14.1 T, vertical wide-bore (89 mm), actively shielded magnet interfaced to an Avance Spectrometer/Imaging console equipped with a micro-imaging gradient system providing a maximum gradient strength of 1000 mT/m and rise time to full amplitude of 110  $\mu$ s (Bruker Biospin, Billerica, Massachusetts, USA). Anesthetized mice were situated in an upright position in a linearly polarized 600 MHz "bird-cage" resonator (26 mm ID, 52 mm length).

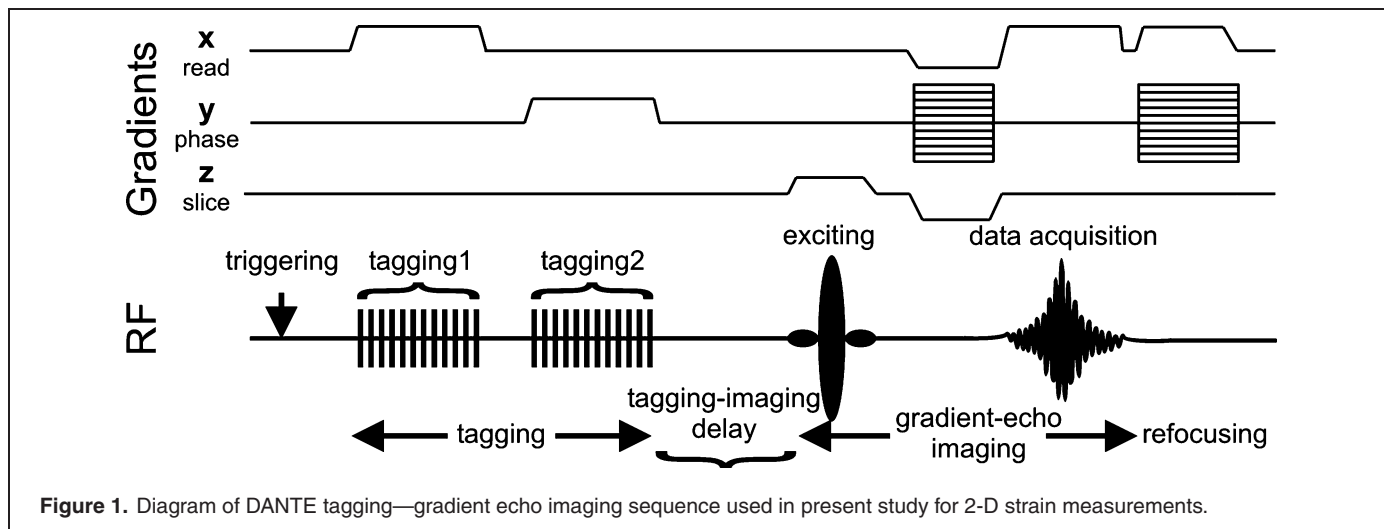
All measurements were preceded by probe tuning and magnet manual shimming. At the start of each experiment, long-axis and transverse plane scout images were taken to localize the position of the heart, determine orientation of the true short axis plane, and identify the time to end-systole. A mid-ventricular short axis slice was located from scout images halfway between the apex and base and corresponding images were acquired. The cardiac main axis offset from the body's principal axis was drastically different for transgenic mice than for wild type and locating of the heart required more scouting images. Control long-axis plane, four chamber images of the heart were acquired every 20–25 minutes to monitor the position of the heart over the entire experimental period.

For volumetric analysis seven to nine anatomical, true short axis contiguous slices (no interslice gap) were taken at end-diastole and end-systole to cover the entire left ventricle. Images were acquired using fast gradient echo (GEFI) with 1000  $\mu$ s sinc excitation pulse, field of view (FOV) 20 mm, slice thickness 1 mm, shortest possible echo time (TE) 1.5 ms, flip angle 90°, acquisition matrix 128  $\times$  128, and number of excitation (NEX) 4. Repetition time (TR) of imaging sequence was selected to be less than RR-interval of fastest beating hearts (for HR = 550 bpm the corresponding RR-interval = 110 ms), so real repetition time corresponds to one cardiac cycle. Due to additional respiratory gating total acquisition time was additionally prolonged by 25–35%, depending on respiration rate.

### *Myocardial tagging*

Tagged images were obtained using a modified DANTE/spin-echo sequence (14), originally developed for selective excitation in FT NMR spectroscopy (15) proved to be capable of producing very narrow tag lines in a relatively short time, thus, making it particularly useful in the study of small animals hearts (16) where fast heart rate and small heart size require high spatial and temporal resolution of tagging. As spin-echo sequences were more susceptible to motion artifacts, fast gradient echo was employed.

The two dimensional tagging grid was generated by two composite pulses consisting of 12 hard pulses, 15  $\mu$ s each, separated by 600  $\mu$ s with corresponding gradients in two



orthogonal directions (Fig. 1). Tagging lines separation was determined by the interpulse delay, and line thickness was determined by the composite pulse length. For a given gradient strength, the length of a single pulse in a sequence determined the tagging region. With tagging gradients of 88 mT/m (less than 10% of maximum gradient strength), the sequence yielded tag grid separation of 0.45 mm (5.8 of  $256 \times 256$  image pixel spacing) and grid line thickness of 0.1 mm. Theoretically, a 6.78 ms composite pulse, consisting of 12 hard  $15 \mu\text{s}$  pulses with  $600 \mu\text{s}$  separation covers the bandwidth of 148 Hz. Gradients of 88 mT/m (37.5 kHz/cm for protons) then enable selective saturation of protons in a 0.04 mm slice. However, with FOV 20 mm, a  $256 \times 256$  acquisition matrix, and corresponding pixel resolution of 0.078 mm, we have produced visible line thicknesses slightly under 0.1 mm (1 image pixel spacing).

Following the tagging period, fast gradient-echo short axis mid-ventricular CINE images were acquired with the following parameters: TR 200 ms (effectively two RR-intervals), TE 1.9 ms, flip angle  $90^\circ$ , acquisition matrix  $256 \times 256$ , NEX 4, temporal separation of 8 ms. Refocusing gradients were applied at the end of the sequence to remove residual spin saturation. A stronger gradient of 120 mT/m was applied for finer tagging resolution ( $0.33 \times 0.33$  mm, 4.2 image pixel spacing) with the same timing using the DANTE sequence.

### Image analysis

Images were processed with a Matlab (MathWorks, Natick, Massachusetts, USA) based program (1, 17). Mid-base wall thickness and volumes were calculated from manually traced epi- and endo-cardial contours on standard short axis gradient echo images taken at end-diastole and end-systole. Regional values of wall thickness and strain myocardium were determined in four segments: septal, anterior, lateral and inferior (18). Tagged images were zero-filled and reconstructed to a  $512 \times 512$  matrix on which tag intersections were manually traced. The reference frame was the first image taken at end-diastole with a minimum tagging-imaging delay (2.2 ms), and the image showing smallest LV chamber volume was assigned as the end-systole frame. Two dimensional homogeneous strain analysis was used for calculations of regional and average principal E1 and E2, and Err and Ecc strains.

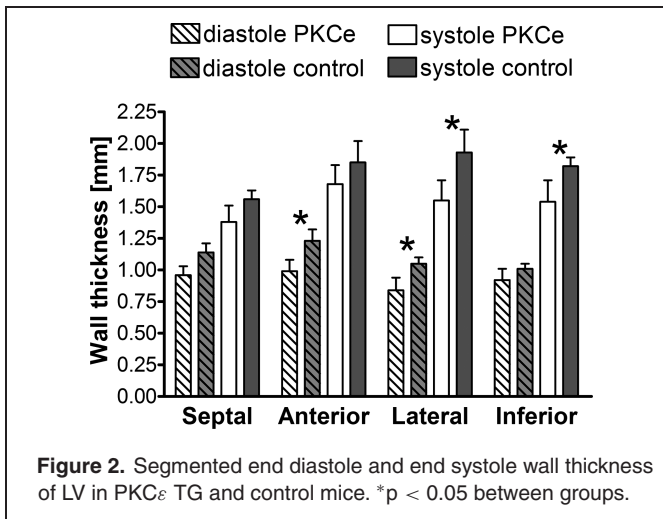
### Statistical analysis

Comparison of global wall thickness and strains between transgenic and control mice was performed using the two-tailed unpaired Student's t-test. Comparison of segmented wall thickness and strains between groups was performed using two-way ANOVA with Bonferroni selected pairs post test. Data are expressed as a mean  $\pm$  standard error at a significance level of  $p < 0.05$ .

**Table 1.** Physiological state and cardiac function.

	Normal FVB/N	Control FVB/N	PKC $\epsilon$
Weight (g)	32.8 $\pm$ 1.6	32.3 $\pm$ 1.6	31.0 $\pm$ 2.3
Heart rate (bpm)	455 $\pm$ 47	497 $\pm$ 34	453 $\pm$ 53
Respiration rate (resp/min)	N/A	78 $\pm$ 15	100 $\pm$ 17*
End diastolic volume [ $\mu\text{l}$ ]	N/A	71 $\pm$ 8	78 $\pm$ 11
End systolic volume [ $\mu\text{l}$ ]	N/A	25 $\pm$ 5	39 $\pm$ 9*
EF (%)	65 $\pm$ 10	66 $\pm$ 3	51 $\pm$ 5*
Diastolic LV wall thickness (mm)	0.98 $\pm$ 0.11	1.11 $\pm$ 0.03	0.93 $\pm$ 0.05*
Systolic LV wall thickness (mm)	1.58 $\pm$ 0.23	1.79 $\pm$ 0.07	1.54 $\pm$ 0.11*

\*P < 0.05 between control FVB/N and PKC $\epsilon$ .



## RESULTS

### Physiologic data

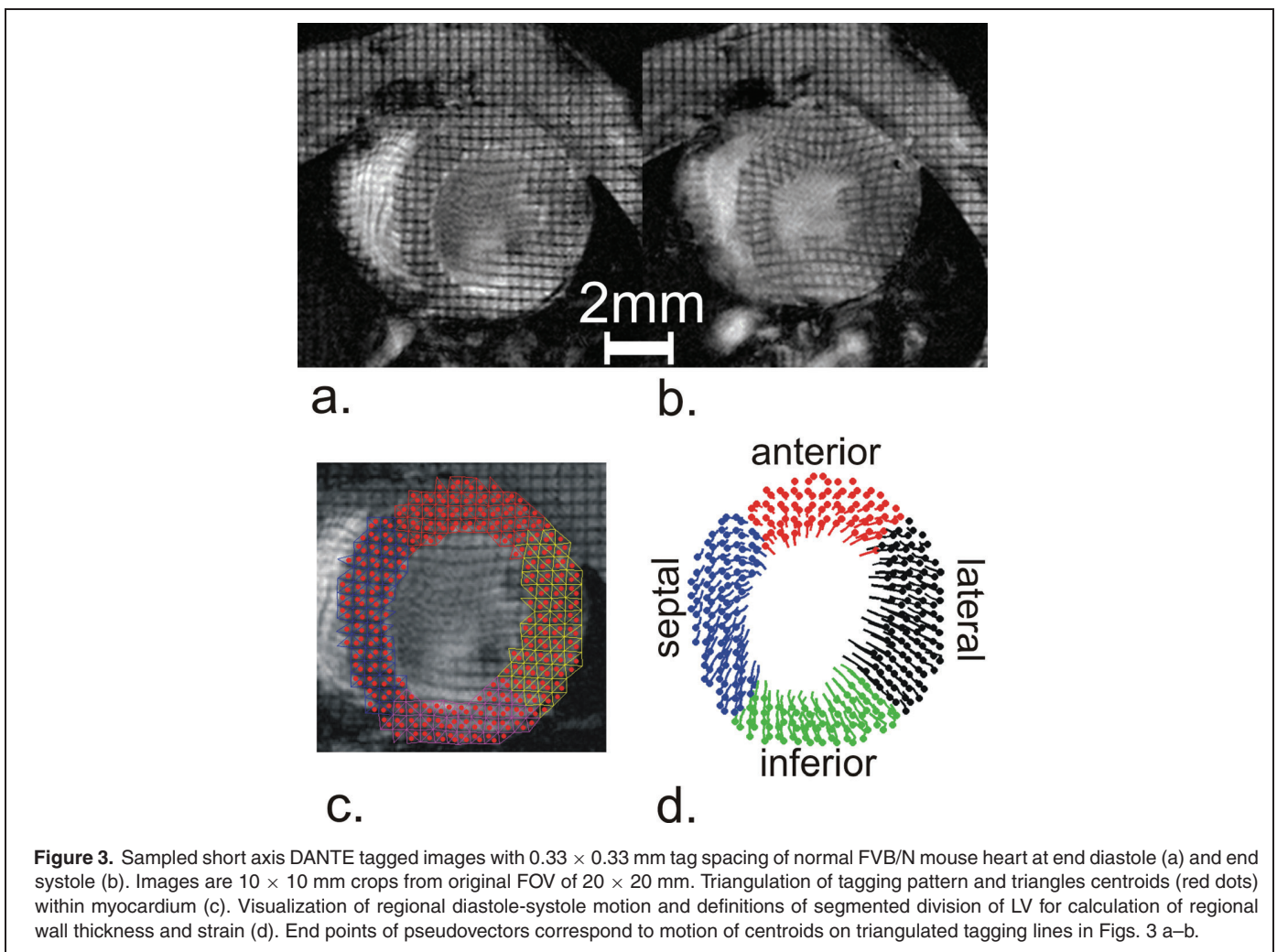
Table 1 summarizes the physiological parameters of all three experimental groups of mice. Heart rates were similar among

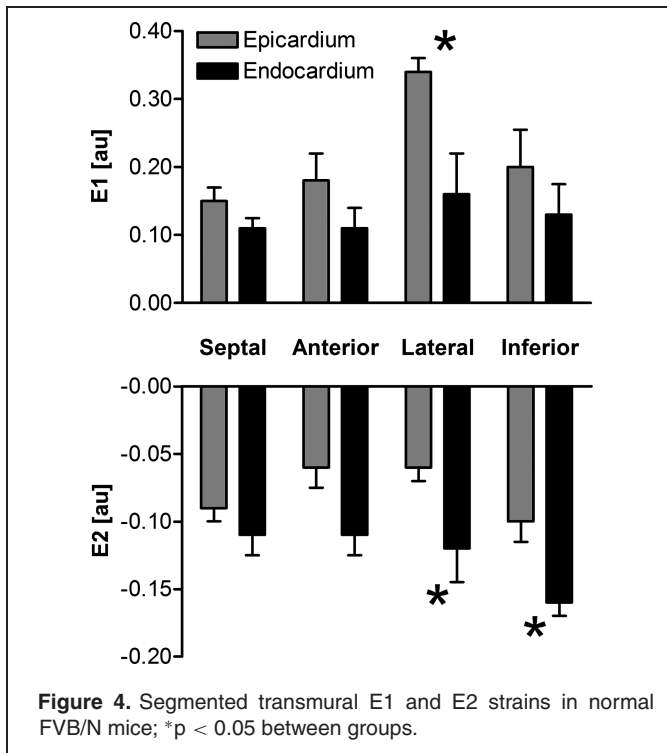
all groups. PKC $\epsilon$  TG mice show higher end-diastolic, and systolic volumes than control mice. Ejection fraction (EF) in normal FVB/N and control FVB/N mice was similar to previously reported values (19–21). As expected, EF was significantly compromised in dilated hearts of PKC $\epsilon$  TG mice. PKC $\epsilon$  TG mice also displayed elevated respiration rates.

At age 9 months, PKC $\epsilon$  TG mice developed thinning of the myocardial wall. The mean end-diastolic LV wall thickness (mid-ventricular level) in PKC $\epsilon$  TG mice was 19% lower than in age-matched controls. At end-diastole, significant thinning of the anterior and lateral segments occurred in PKC $\epsilon$  TG (Fig. 2). At end-systole, the lateral and inferior segments of the hearts in PKC $\epsilon$  TG were the most compromised, compared to septal and anterior segments (Fig. 2).

### Transmural tagging measurements

Figure 3a–b show tagged end-diastole and end-systole images with a grid size of 0.33  $\times$  0.33 mm. This fine grid resolution provided three to five pairs of centroids across the wall (Fig. 3c) and enabled transmural measurements of E1 and E2 for the comparison of epicardial and endocardial strains in



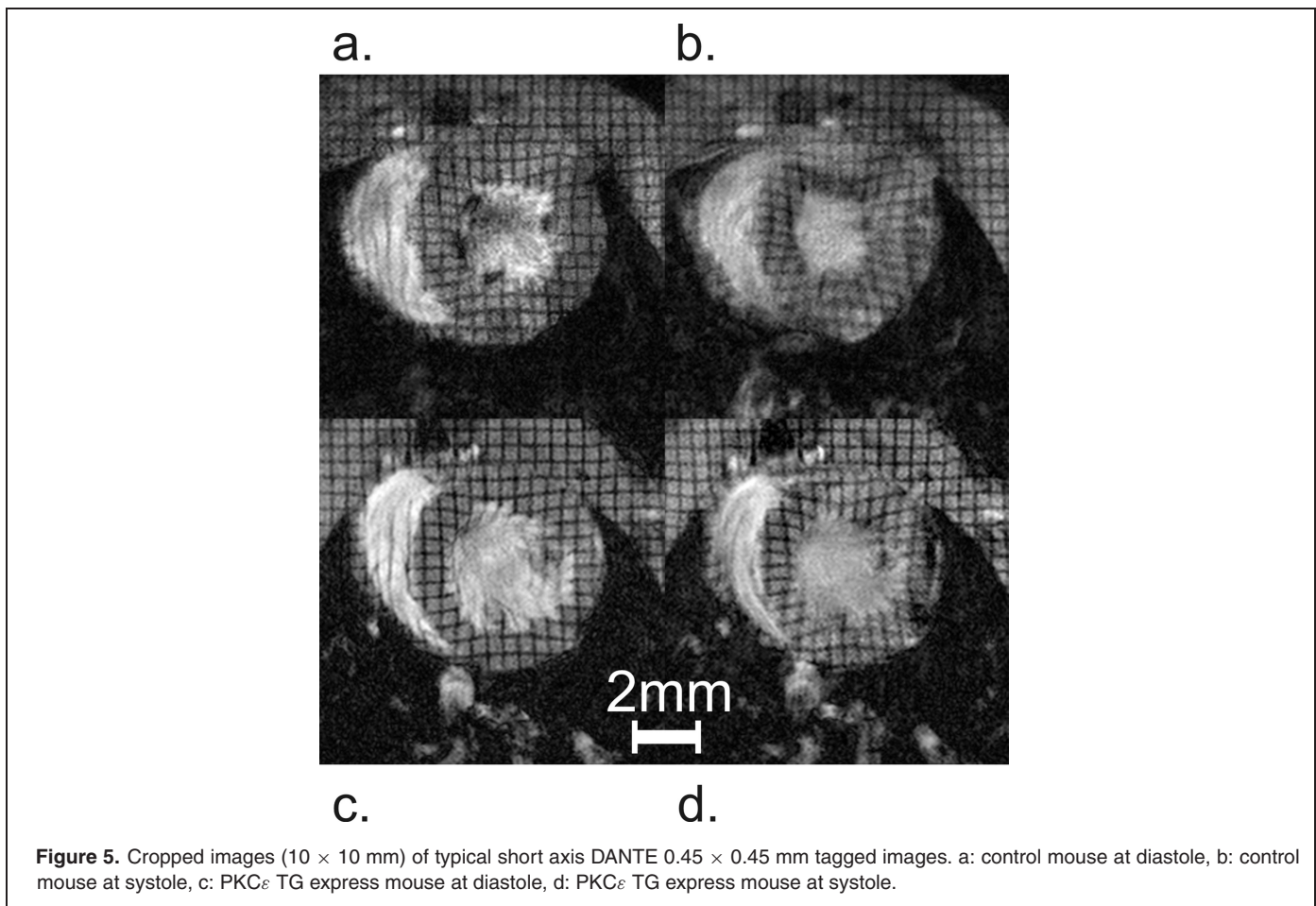


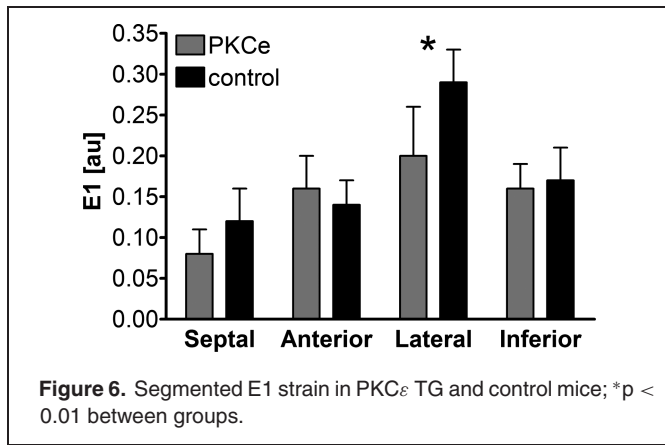
the normal myocardium. Visualization of motion of centroids is shown on Fig. 3 d.

Figure 4 presents measurements of epi- and endocardial E1 and E2 in normal hearts of FVB/N mice obtained with a  $0.33 \times 0.33$  mm tagging grid. Stretch in each segment was higher in the epicardial layer, while compression was higher in the endocardial layer. The lateral segment, which accommodated 4–6 tagging intersections, demonstrated significant transmural distinctions in principal strains. Averaged over all four segments, mean epicardial E1 was 69% higher than the endocardial E1 (epi =  $0.22 \pm 0.10$ ; endo =  $0.13 \pm 0.07$ ,  $p < 0.05$ ). However, magnitude of mean endocardial E2 was 50% greater than E2 in the epicardium (endo =  $-0.12 \pm 0.03$ , epi =  $-0.08 \pm 0.03$ ;  $p < 0.001$ ).

### Strain in dilated cardiomyopathy

Representative images of control and PKC $\epsilon$  TG mice tagged with  $0.45 \times 0.45$  mm lines at both diastole and systole are shown in Fig. 5. Cardiac images of PKC $\epsilon$  TG mice show wall thinning in the lateral segment. Magnetic resonance imaging at ultra-high fields is prone to artifacts caused by susceptibility effects (22). The lateral segment on Fig. 5d shows little loss of the signal in the region of local field inhomogeneities. Use of the shortest available TE (1.9 ms) and extensive shimming reduced this





**Figure 6.** Segmented E1 strain in PKCε TG and control mice; \*p < 0.01 between groups.

effect. If signal loss significantly effected the LV area, imaging was repeated with new shimming values. Smaller contraction at systole is also visible as is consistently with reduced EF measurements in PKCε TG mice (Table 1). At least two tag intersections populate the LV wall in all segments providing sufficient resolution for accurate E1 and E2 principal strain calculations despite significant wall thinning (Table 1). The tagging lines on end-diastole images (Figs. 5a and 5c) that are used as reference in strain calculations are affected by a “finite” tagging time and show signs of radically inward oriented bending around the whole circumference. For hearts beating at 500 bpm, the R-R interval is 120 ms and a 14 ms tagging period constitutes a significant amount of time for the myocardium to evolve, leading to deformation of tagging lines on the reference images. We lowered this deformation by triggering the scanner at the rising slope of R wave. The contrast-to-noise ratio between the tags and myocardium changed less than 10% over the end-diastole to end-systole interval.

End systolic regional E1 strains are summarized in Fig. 6. Control E1 in the lateral segment was elevated in comparison to the other segments (p < 0.05). In the dilated hearts of the PKCε TG mice, the septal segment displayed the lowest value of E1 (p < 0.05). In comparison to controls, E1 in the septal and lateral segments of dilated, PKCε TG hearts was reduced by 33% and by 31% (p < 0.01), respectively. Also, global E1, averaged over all segments, was significantly reduced in the thinned LV walls of dilated heart (PKCε TG = 0.14 ± 0.02; control = 0.18 ± 0.02, p < 0.01). E2 was similar in all segments of both groups at approximately -0.11 ± 0.01.

Magnitudes of radial and circumferential strains and absolute values of prime angle are presented in Table 2 and do not show significant differences between both groups.

## DISCUSSION AND CONCLUSIONS

We report here the first measurements of regional principal strains in the thinned left ventricular wall of a dilated murine mouse heart. This study of dilated cardiomyopathy was facilitated by significant improvements in spatial resolution over that of previous efforts to measure E1 and E2 in the left ventricle by conventional tagging (2). With the combination of ultra-high magnetic field, high magnetic gradients, and cardiac and respiratory gating, the DANTE method produced tagging grids on anatomical images with the resolution as high as 0.33 × 0.33 mm.

The results show that at the mid-ventricular level, the thinned lateral and septal walls of the PKCε TG mouse exhibited significantly lower E1 strain, associated with stretch, than in the control myocardium. This finding is consistent with the impaired contractile performance of the dilated heart. However, the fact that global and regional principal strains E2 in control and PKCε G groups remain essentially unchanged is intriguing suggests that the strain associated with compression is not compromised in the dilated myocardium, and may be more likely connected to a hypertrophic than dilated phenotype.

Differences in Err and Ecc strains of control and PKCε TG were not detected. This finding is not surprising given the wide regional distribution of prime angles (Table 2) that lowers and adds additional variation to the strain magnitude in hearts with similar E1 or E2. Clearly, the first principle strain E1 is a more sensitive parameter to distinguish small differences in regional strains of normal and thinning LV than radial and circumferential strain.

Using DENSE method in normal mice hearts, higher values for Err and Ecc have been reported (9). We speculate that, apart from applying a faster method, the difference in obtained strain values may also originate from a slight offset in the long-axis of midventricular slices in both studies. Indeed, the reported values of Err in 1 mm slices that were separated only by 0.5 mm drop from 0.30 ± 0.05 in midventriculum to 0.16 ± 0.05 in apex.

High resolution tagging with 0.33 mm line separation and 0.1 mm line thickness was achieved to permit more accurate sampling of the mouse ventricular wall. In terms of 0.078 mm

**Table 2.** Mean regional and global values of radial and circumferential strains, and absolute values of prime angles (Θ) in LV of control FVB/N and PKCε mice. Data are presented as mean ± standard deviation. No intra-group and between groups differences were detected.

Region	Control FVB/N			PKCε		
	Err	Ecc	Θ[°]	Err	Ecc	Θ[°]
Septal	0.07 ± 0.03	-0.05 ± 0.03	8.5 ± 7.3	0.04±0.03	-0.06 ± 0.01	12.7 ± 7.0
Anterior	0.08 ± 0.01	-0.05 ± 0.01	6.4 ± 3.5	0.11±0.05	-0.05 ± 0.01	11.0 ± 5.4
Lateral	0.17 ± 0.06	-0.05 ± 0.01	12.6 ± 5.6	0.20±0.07	-0.06 ± 0.03	10.2 ± 4.2
Inferior	0.12 ± 0.05	-0.05 ± 0.02	4.3 ± 3.6	0.12±0.07	-0.04 ± 0.02	4.7 ± 2.5
Global	0.11 ± 0.02	-0.05 ± 0.01	1.1 ± 0.8	0.11±0.03	-0.05 ± 0.01	2.7 ± 1.3

image resolution, 0.33 mm tagging results in tag line spacing of 4 pixels and a line thickness of 1 pixel. This resolution enabled the first transmural strain measurements in the normal mouse heart using a spin saturation tagging method and elucidated significant differences in E1 and E2 between the epicardial and endocardial layers. These differences are consistent with the known relative extents of wall thickening in the endocardial and epicardial layers reported for humans. Indeed, previous studies also demonstrate reductions in sub-epicardial E2 compared to epicardial E2 in human hearts, as shown here for mouse heart (23, 24). Transmural gradients of E1 and Err data in (23) are not available due to stated limitations in spatial tagging resolution in the radial direction. Direct comparison of absolute values of strains between human and mouse hearts is confounded by the extreme differences in heart rate and LV dimensions (1).

Although some published data shows that systolic sub-endocardial thickening is substantially greater than sub-epicardial thickening (25, 26), there are contradicting reports that indicate near-uniform transmural thickening in canine LV (27). In addition, Cheng et al. (28, 29) observed an absence of transmural gradients in both regional wall thickening and regional first principal strain in the ovine LV. Therefore, the experimental heart model (i.e., species) and methods for strain measurement appear to influence the relative principal strain values for the epicardium and endocardium.

Mean values of systolic principal E1 obtained by DANTE tagging for the control group with similar heart rates are slightly smaller at  $0.18 \pm 0.02$  than previously reported values by Zhou et al. (2) in normal mice generated from SPAMM tagging methods at  $0.22 \pm 0.08$  but well within experimental error. The potential difference across methods may be due to the faster generation of the tagging grid using SPAMM (10 ms), but at the cost of significantly reduced tagging resolution: SPAMM separation/thickness = 0.7/0.2 mm vs DANTE separation/thickness = 0.45/0.1 mm).

There is little published data on E2 strain in the mouse heart. The current E2 values ( $0.11 \pm 0.01$ ) are within experimental error of previously reported regional values of E2 ( $-0.15 \pm 0.08$  and  $-0.17 \pm 0.06$ ) from SPAMM data (2). Using a faster DENSE method, Gilson et al. report an average E2 value of  $-0.21$ , but unfortunately offer no information on measurement variability (4).

In our study on mouse hearts, a strong relationship exists between calculated strain values and heart rate. When heart rate is elevated from 380 bpm to 500 bpm, calculated strain values are generally reduced 15–20%. There are three reasons for lower end-systolic strain measurements: the tagging grid is not generated precisely at end-diastole due to R-wave detection delays and internal delays within the sequence; tagging grid distortion due to tag long encoding time; and tagging grid evolves during reference image acquisition due to long acquisition time. All three factors contribute when heart rates approach 400 bpm. However, fast gradient echo essentially eliminates the influence of image acquisition time on strain values. As present technology does not provide simultaneous fast and fine tagging, a fundamental question arises: what conditions for

tag generation are required for strain measurements in the fast beating, small hearts of mice: higher spatial or higher temporal resolution? Definitely, lower temporal resolution delivers lower strain values, but lower spatial resolution measurements produce higher errors, particularly in E1 and Err strains, and can not provide transmural strain measurements across the LV wall. Therefore, for the purposes of this study, we justify using higher spatial resolution at the cost of temporal resolution.

Importantly, Wiesman et al. reported no significant differences in hemodynamic values obtained from either horizontal or vertical positioning of mice (30). However, this is the first report of principal strain measurements conducted in vertical bore magnets. Although the first 3D motion mapping of murine myocardium with phase-contrast MRI in ultra-high 17.6 T vertical bore magnet has been published (31), it does not offer strain related data. To date, the consequences of prolonged upright body position in anesthetized animals on cardiac strain measurements remain purely speculative. Interestingly, concerns regarding the horizontal versus vertical positioning in animals are seldom applied regarding the routine examination of humans in the supine position.

In summary, high spatial resolution myocardial tagging at 14.1 T provided new insight into the functional utility of the ever-increasing role for murine mouse models of cardiac disease and, as shown here, LV wall dynamics. The ability to discern principal strain differences between the endocardial and epicardial layers in the mouse LV indicates the use of cardiac tagging for integrated studies of newly emerging molecular models of contractile filament modification (10, 32).

## REFERENCES

1. Wei L, Ashford MW, Chen J, Watkins MP, Williams TA, Wickline SA, Yu X. MR tagging demonstrates quantitative differences in regional ventricular wall motion in mice, rats, and men. *Am J Physiol Heart Circ Physiol* 2006;291:H2515–21.
2. Zhou R, Pickup S, Glickson JD, Scott CH, Ferrari VA. Assessment of global and regional myocardial function in the mouse using Cine and tagged MRI. *Magn Reson Med* 2003;49:760–4.
3. Heijman E, Strijkers GJ, Habets J, Janssen B, Nicolay K. Magnetic resonance imaging of regional cardiac function in the mouse. *MAGMA* 2004;17:170–8.
4. Gilson WD, Yang Z, French BA, Epstein FH. Complementary displacement-encoded MRI for contrast-enhanced infarct detection and qualification of myocardial function in mice. *Magn Reson Med* 2004;51:744–52.
5. Wu EX, Towe CW, Tang H. MRI cardiac tagging using a sinc-modulated RF pulse train. *Magn Reson Med* 2002;48:389–93.
6. Epstein FH, Yang Z, Gilson WD, Berr SS, Kramer CM, French BA. MR tagging early after myocardial infarction in mice demonstrates contractile dysfunction in adjacent and remote regions. *Magn Reson Med* 2002;48:399–403.
7. Henson RE, Song SK, Pastorek JS, Ackerman JJH, Lorenz CH. Left ventricular torsion is equal in mice and humans. *Am J Physiol Heart Circ Physiol* 2000;278:H1117–23.
8. Aletras AH, Ding S, Balaban RS, Wen H. DENSE: displacement encoding with stimulated echoes in cardiac functional MRI. *J Magn Reson* 1999;137:247–252.

9. Gilson W D, Yang Z, French BA, Epstein FH. Measurements of myocardial mechanics in mice before and after infarction using multislice displacement-encoded MRI with 3D motion encoding. *J Physiol Heart Circ Physiol* 2005;288:H1491–7.
10. Goldspink PH, Montgomery DE, Walker LA, Urboniene D, McKinney RD, Geenen DL, Solaro RJ, Buttrick PM. Protein kinase C epsilon overexpression alters myofilament properties and composition during the progression of heart failure. *Circ Res* 2004;95:424–32.
11. Scruggs SB, Walker LA, Lyu T, Geenen DL, Solaro RJ, Buttrick PM, Goldspink PH. Partial replacement of cardiac troponin I with a non-phosphorylatable mutant at serines 43/45 attenuates the contractile dysfunction associated with PKC $\epsilon$  phosphorylation. *J Mol Cell Cardiol* 2006;40:465–73.
12. Schneider JE, Cassidy PJ, Lygate C, Tyler DJ, Wiesmann F, Grieve SM, Hulbert K, Clarke K, Neubauer S. Fast, High-resolution in vivo Cine magnetic resonance imaging in normal and failing mouse hearts on a vertical 11.7T system. *J Magn Reson Imaging* 2003;18:691–701.
13. Cassidy PJ, Schneider JE, Grieve SM, Lygate C, Neubauer S, Clarke K. Assessment of motion gating strategies for mouse magnetic resonance at high magnetic fields. *J Magn Reson Imaging* 2004;19:229–37.
14. Mosher TJ, Smith MB. A DANTE tagging sequence for the evolution of translational sample motion. *Magn Reson Med* 1990;15:334–9.
15. Morris GA, Freeman R. Selective excitation in Fourier transform nuclear magnetic resonance. *J Magn Reson* 1978;29:433–62.
16. De Crespigny AJS, Carpenter TA, Hall LD. Cardiac tagging in the rat using a DANTE sequence. *Magn Reson Med* 1991;21:151–6.
17. Liu W, Chen J, Ji S, Allen JS, Bayly PV, Wickline SA, Yu X. Harmonic phase magnetic resonance imaging tagging for direct quantification of Lagrangian strain in rat hearts after myocardial infarction. *Magn Reson Med* 2004;52:1282–90.
18. Cerqueira MD, Weissman NJ, Dilsizian V, Jacobs AK, Kaul S, Laskey WK, Pennell DJ, Rumberger JA, Ryan T, Verani MS. Standardized myocardial segmentation and nomenclature for tomographic imaging of the heart. *Circulation* 2002;105:539–42.
19. Ruff J, Wiesmann F, Hiller K-H, Voll S, von Kienlin M, Bauer WR, Rommel E, Neubauer S, Haase A. Magnetic resonance microimaging for noninvasive quantification of myocardial function and mass in the mouse. *Magn Reson Med* 1998;40:43–8.
20. Wiesmann F, Ruff J, Hiller K-H, Rommel E, Haase A, Neubauer S. Developmental changes of cardiac function and mass assessed with MRI in neonatal, juvenile, and adult mice. *Am J Physiol Heart Circ Physiol* 2000;278:H652–7.
21. Williams S-P, Gerber H-P, Giordano FJ, Peale Jr FV, Bernstein LJ, Bunting S, Chien KR, Ferrara N, van Bruggen N. Dobutamine stress Cine-MRI of cardiac function in the hearts of adult cardiomyocyte-specific VEGF knockout mice. *J Magn Reson Imaging* 2001;14:374–82.
22. Herold V, Morechel P, Faber C, Rommel E, Haase A and Jakob PM. In vivo quantitative three-dimensional motion mapping of the murine myocardium with PC-MRI at 17.6T. *Magn Reson Med* 2006;55:1058–64.
23. Moore CC, Lugo-Olivieri, McVeigh ER, Zerhouni EA. Three-dimensional systolic strain patterns in the normal human left ventricle: Characterization with tagged MR imaging. *Radiology* 2000;214:453–66.
24. MacGowan GA, Shapiro EP, Azhari H, Siu CO, Hees PS, Hutchins GM, et al. Noninvasive measurement of shortening in the fiber and cross-fiber directions in the normal human left ventricle and in idiopathic dilated cardiomyopathy. *Circulation* 1997;96:535–41.
25. Gascho JA, Copenhaver GL, Heitjan DF. Systolic thickening increases from subepicardium to subendocardium. *Cardiovasc Res* 1990;24:777–80.
26. Costa KD, Takayama Y, McCulloch AD, Covell JW. Laminar fiber architecture and three-dimensional systolic mechanics in canine ventricular myocardium. *Am J Physiol Heart Circ Physiol* 1999;276:H595–607.
27. Hittinger L, Shannon RP, Kohin S, Manders WT, Kelly P, Vatner SF. Exercise-induced subendocardial dysfunction in dogs with left ventricular hypertrophy. *Circ Res* 1990;66:329–43.
28. Cheng A, Langer F, Rodriguez F, Criscione JC, Daughters GT, Miller DC et al. Transmural cardiac strains in the lateral wall of the ovine left ventricle. *Am J Physiol Heart Circ Physiol* 2005;288:1546–56.
29. Cheng A, Langer F, Rodriguez F, Criscione JC, Daughters GT, Miller DC, et al. Transmural sheet strains in the lateral wall of the ovine left ventricle. *Am J Physiol Heart Circ Physiol* 2005;289:1234–41.
30. Wiesmann F, Neubauer S, Haase A, Hein L. Can we use vertical bore magnetic resonance scanners for murine cardiovascular phenotype characterization? Influence of upright body position on left ventricular hemodynamics in mice. *J Cardiovasc Magn Reson* 2001;3:311–15.
31. Herold V, Moerchel P, Faber C, Rommel E, Haase A, Jakob PM. In vivo quantitative three-dimensional motion mapping of the murine myocardium with PC-MRI at 17.6T. *Magn Reson Med* 2006;55:1058–64.
32. Urboniene D, Dias FA, Pena JR, Walker LA, Solaro RJ, Wolska BM. Expression of slow skeletal troponin I in adult mouse heart helps to maintain the left ventricular systolic function during respiratory hypercapnia. *Circ Res* 2005;97:70–7.